Research Square

Preprints are preliminary reports that have not undergone peer review.
They should not be considered conclusive, used to inform clinical practice,
or referenced by the media as validated information.

# Design and simulation of engineered Josephson parametric amplifier in quantum two-mode squeezed radar

**Milad Norouzi**
Vali-e-Asr University of Rafsanjan
**Seyed M. Hosseiny** ( sm.hosseiny@urmia.ac.ir )
University of Urmia
**Jamileh Seyed-Yazdi** ( j.seyedyazdi@gmail.com )
Vali-e-Asr University of Rafsanjan https://orcid.org/0000-0002-7345-2142
**Mohammad H. Ghamat**
University of Shiraz

**Research Article**

**Keywords:** Engineered JPA, Quantum illumination, Quantum correlation, QTMS radar, SNR.

**Posted Date:** August 11th, 2022

**DOI:** https://doi.org/10.21203/rs.3.rs-1948219/v1

**License:** This work is licensed under a Creative Commons Attribution 4.0 International License.
Read Full License

# Design and simulation of engineered Josephson parametric amplifier in quantum two-mode squeezed radar

Milad Norouzi[1], Seyed M. Hosseiny[2]*, Jamileh Seyed-Yazdi[1]*, Mohammad H. Ghamat[3]

[1]Department of Physics, Faculty of Science, Vali-e-Asr University of Rafsanjan, Rafsanjan, Iran.

[2]Department of Physics, Faculty of Science, University of Urmia, Urmia, Iran.

[3]Electrical Engineering Department, University of Shiraz, Shiraz, Iran.

The authors M.N. and S.M.H. contributed equally to this work.

*Email: j.seyedyazdi@gmail.com, sm.hosseiny@urmia.ac.ir

## Abstract

Josephson parametric amplifier (JPA) engineering is a significant component in the quantum two-mode squeezed radar (QTMS), to enhance, for instance, radar performance and the detection range or bandwidth. In this study, we apply quantum theory to a research domain focusing on the simulation of QTMS radar. We simulate a proposal of using engineered JPA (EJPA) to enhance the performance of a QTMS radar. We define the signal-to-noise ratio (SNR) and detection range equations of the QTMS radar. The engineered JPA leads to a remarkable improvement of the quantum radar performance, i.e. a large enhancement in SNR of about 6 dB more than the conventional QTMS radar (with respect to the latest version of QTMS radar, and not to classical radar), a substantial improvement in the probability of detection through far fewer channels. Finally, we simulate signal transmission to target in QTMS radar and achieve a huge increase in QTMS radar range, from half a meter in the conventional JPA to 482 m in the current study.

**Keywords**: Engineered JPA, Quantum illumination, Quantum correlation, QTMS radar, SNR.

## 1. Introduction

In general, radars transmit radio waves to one or more targets using transmitter antennas and receive and measure echoes using receiver antennas to detect the presence or absence of targets by a detector. Many factors, such as noise and clutter, can be mentioned that call into question this

simplicity [1]. The difference between a quantum radar (QR) and a classical radar (CR) can be deduced even from their names. Basic quantum concepts such as the principle of uncertainty, entanglement, correlation, photon statistics, vacuum fluctuations, and squeezing are present in QRs [1-19]. The discussion about QRs has flourished for several years. Several research teams, including Balaji et al. [1-3], Barzanjeh et al. [15], etc., have implemented operational prototypes of QR. All the results obtained by these teams show a significant improvement in the performance of QR compared to the CR counterpart [2-9, 15, 19]. A 6 dB improvement in transmission power [11], 4 to 6 dB enhancement in SNR [2-9, 15, 19, 20], and an improvement of 6 dB in the QR Receiver Operating Characteristic (ROC) curve [19, 20] compared to CR can be considered. The quantum illumination (QI) range, which gives the accuracy of the square of the mean of the delay of range, can be tens of dB above that of a CR counterpart with the same bandwidth and transmitted energy [20]. In the QR, the samples are much fewer than in the CR, and the signal in QR has a higher correlation coefficient than its classical counterpart [2-9, 15, 19]. The QRs can also be made impervious to hackers by using quantum cryptography [9]. This means that it is possible to create a secure channel by encoding the transmitted photons to protect the information against eavesdropping [9]. The target may also be more visible by using QR rather than CR, due to a quantum effect on the radar cross-section [21]. One type of QR is the quantum two-mode squeezed (QTMS) radar, which is very similar to conventional noise radars [1-3]. These radars use the Josephson parametric amplifier (JPA) and can produce the signal and idler directly in the microwave band [1-3, 6, 8, 11, 12, 15, 16]. On the other hand, one of the current disadvantages of QTMS radars is their very high costs of implementation and equipment [1-3, 6, 8, 11, 12, 15, 16]. In recent articles [1-3, 6, 8, 11, 12, 15] it was observed that JPAs have limitations such as low bandwidth and therefore, we need to engineer them to improve the performance of the QR. Hence,

engineering JPAs in QTMS radars, gives us the capabilities to build high-range QTMS radars. One of the most important issues for engineers is the range measurement of a QR. Therefore, in this study, the range equation of a QTMS radar is introduced and the results are reviewed. We simulate a QTMS radar proposal with larger bandwidth, better detection range, and improved SNR, taking into account the prototype of the QTMS radar implemented in [1, 3] and using the EJPA [22]. The QTMS radar has shown much more enhancement from classical than 6 dB [2-9, 15, 19, 20], and this paper purports to have an additional 6 dB from those results. In this work, we present a simulation study of a QR inspired by quantum illumination, which requires only independent measurement of the signal and idler. After introducing QR and the basic principles of the QTMS radars, we present and evaluate the EJPA and use it to simulate the radar's design. Finally, after post-processing, the results are presented to show and confirm the capability of our design.

# 2. Preliminaries

### 2.1. Quantum Radar (QR)

The basis of the work of a QR can be summarized as follows [1-19]:

1. Using a pump and a signal generator, we produce a current of entangled photon pairs (signal/idler) by quantum sources.

2. To send a signal to the target, we need to amplify the signal with low-noise amplifiers, and to determine the presence of the target, we have to record the idler.

3. After receiving the signal reflected from the target by the receiver antenna, the signal and idler are amplified again, and apply a match-filtering between the received signal and the previously recorded idler.

4. Using a suitable detector, the presence or absence of a target can be inferred. Fig. 1 depicts the general block diagram of a quantum radar.

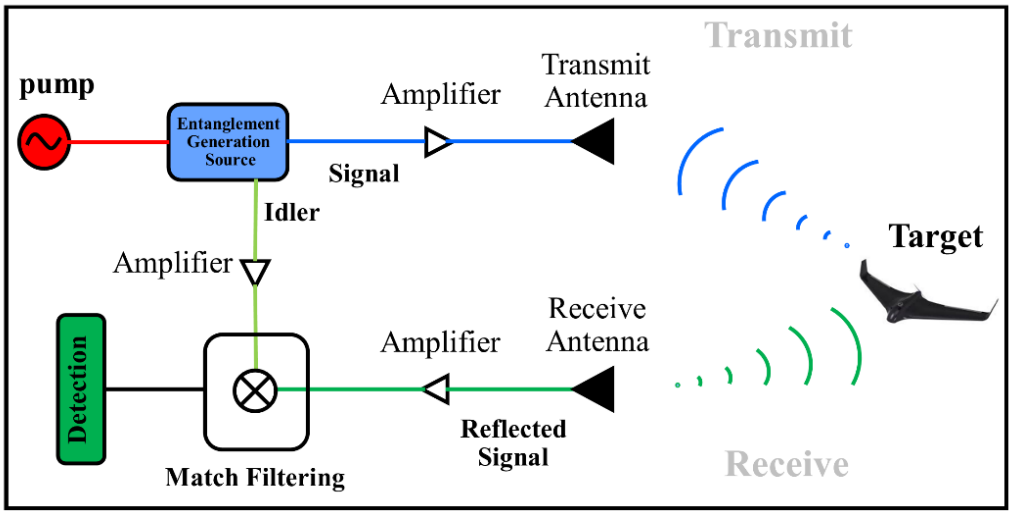


Fig. 1. Schematic block diagram of a QR.

### 2.1.1. QTMS Radar

The template is used to as mentioned, a type of QRs is the quantum two-mode squeezed (QTMS) radar, the operational prototype of which was introduced in [1-3, 5, 6, 8, 15]. Here, the term squeezed refers to the electromagnetic field state that decreases the uncertainty of one component of the field relative to the coherent state (uncertainty in the amplitude and phase of the electric field are the same), increasing uncertainty in the other component [1, 3]. The wave packet, in another word, is compressed or squeezed inside a potential well [23], or, to be more precise,

quantum noise decreases in linear compounds of some of the quadrature and increases in other compounds [1-3, 5, 6, 8].

The main part of QTMS radars is the source of entanglement generation, the Josephson parametric amplifier (JPA). JPAs are devices that generate a two-mode squeezed vacuum (TMSV) state [1-3, 5, 6, 8]. The term vacuum here refers to vacuum or zero-point energy-related fluctuations, which we intend to amplify. These fluctuations are not similar to classical ones [1, 3]. When the field is quantum, in an absolute vacuum, particles can fluctuate, and these fluctuations lead to spontaneous emission from an excited state at an energy level to the ground state at the energy level , thus emitting a photon with an energy equal to the difference between these two levels, [1-3, 5, 6, 8, 23]. JPAs are placed in dilution refrigerators for two reasons: first, because they have a resonant cavity with a superconducting quantum interferometer (SQUID) and superconducting properties, and second, to prevent noise absorption in the entangled signal [1-3, 5, 6, 8, 15]. Fig. 2 shows a schematic representation of the JPA.

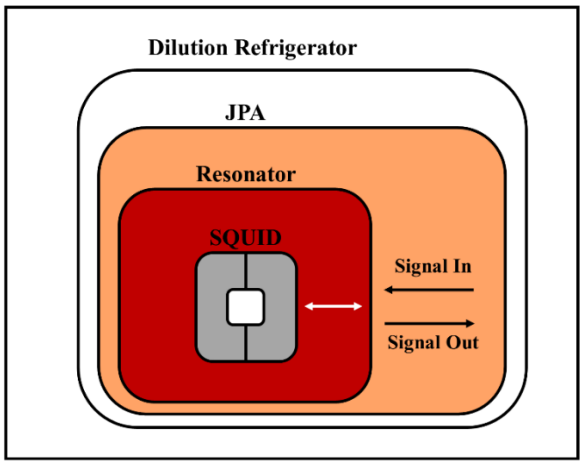


Fig. 2. Schematic representation of a JPA in a dilution refrigerator.

### 2.2. Two Photon Entanglement

A covariance matrix is a matrix whose elements show a correlation between different system parameters. A special type of correlation is entanglement [24-26]. When two beams of light are entangled, they have very strong correlations. The correlation power resulting from quantum entanglement simply cannot occur in classical physics [1, 3]. The root of entanglement is in the quantum superposition principle and has no classical counterpart [26]. In general, in a quantum state, if the measurement on the first qubit affects the result of the measurement of the second qubit, we have an entangled state. Otherwise, it is non-entangled [24, 26].

Since the photons of the signal and idler originate from the same pump photon, there is a strong quantum correlation between the signal and idler, resulting in the squeezing of conjugate signals I and Q [1-3, 5, 6, 8, 15]. For better detection and measurement with classical instruments, the signal and idler need to be amplified in stages. Unfortunately, amplification adds a lot of noise and weakens the entanglement. Entanglement can easily be eliminated by factors such as loss (e. g. antenna gain) and noise (e. g. the presence of amplifiers) [13, 27-29]. However, as shown in experimental results [1], there is a quantum enhancement (in the form of higher correlations) in QTMS radar. The difference between QRs is in the source of their Entanglement. There are different types of entanglement, for example, polarization entanglement [7, 19], number of photons [19], superconductivity (Josephson junctions) [1-3, 5, 6, 8, 15], squeezed light [1-3, 5, 6, 8], quantum dot [29 and 28] and etc. There are also two types of continuous-variable entanglement such as voltage and discrete variables such as polarization [1-3, 5, 6, 8, 15]. In QTMS radars, we utilized the entanglement of continuous variables of light squeezed by the JPA entanglement generation source [1-3,30].

# 3. Results and Discussion

### 3.1. Engineering JPA (EJPA)

The JPAs are commonly used as a narrowband signal amplifiers, meaning that they have limitations (i.e. narrow bandwidth) that prevent the improvement of their performances [1-3, 5, 6, 8, 15, 22]. Our EJPA is similar to that described in [22], where a broadband EJPA by the pumped flux impedance method is presented. Therefore, we use it to construct the quantum radar. One of the advantages of this JPA is the wide bandwidth at low gain rates [22]. By matching the impedance with the input amplifier, its bandwidth is significantly increased from 1 MHz to 300 MHz. The input signal is reflected as an amplified output signal with a gain of about 20 dB [22]. Fig. 3 shows a schematic representation of the equivalent circuit of an EJPA device, in which the entire device is fabricated integrally on intrinsic silicon (>10 kΩcm resistivity). The device operates in a dilution refrigerator with a base temperature of 7 mK [22]. A SQUID loop is made with two Josephson junctions placed in parallel on each side. If the flux line on the chip is combined with two Josephson junctions, flux pumping is provided. The λ/4 resonator with a characteristic impedance of 45 Ω reduces the JPA resonant quality factor. On the other hand, the λ/2 resonator with a characteristic impedance of 80 Ω reduces the frequency dependence in the system sensitivity matrix, and this leads to amplification of the bandwidth [22].

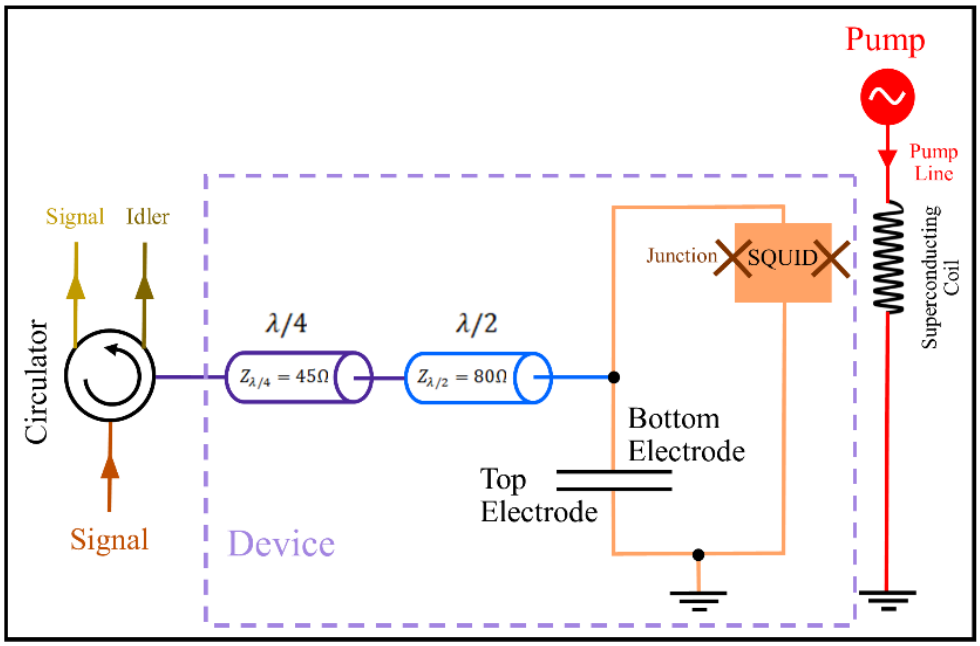


Fig. 3. Schematic representation of an EJPA circuit.

A parallel plate capacitor with two top and bottom electrodes with a total input capacity c = 2.03 ± 0.02 pF is located at the JPA input which is connected to the ground. The input line is galvanically connected to the lower electrode by impedance, which is directly connected to the SQUID. The upper electrode of the capacitor is connected to the ground in parallel with the SQUID with a non-galvanic connection. By connecting galvanic to the input, the coupling quality coefficient decreases, and therefore, the amplification bandwidth increases [22]. The JPA used in the current study is the degenerate four-wave type which means that the input and output frequencies are identical. The signal (and idler) frequency here is 5.31 GHz [22].

### 3.2. A Proposed QTMS Radar Design with EJPA

The block diagram of QTMS Radar is illustrated in Fig. 4. The JPA bandwidth is increased from 1 MHz [1, 3] by the pumped flux impedance method, to 300 MHz. The pump power is 5 dBm. The JPA is located inside the refrigerator, as shown in Fig. 4, and is connected to the T-bias via a

microwave switch (which can turn the pump on or off) and a device called a Shot-Noise Tunnel Junction (SNTJ). These are used as part of the calibration process to confirm the entanglement of the JPA output signal [1-3, 5, 6, 8]. The output signal is amplified to make it easier to measure and detect. Because amplifiers add noise to the signal, and usually the added noise is from the first amplifier, we use a high-electron-mobility transistor (HEMT) (which is a low-noise amplifier) and a semiconductor amplifier [1-3, 5, 6, 8, 15]. HEMT is also placed in a dilution refrigerator and semiconductor amplifiers operate at 4 K. The Bluefors LH250, which uses liquid helium for cooling, is used in experiments in which the cooling power of this refrigerator for a temperature of 7 mK is about 10 μW [31].

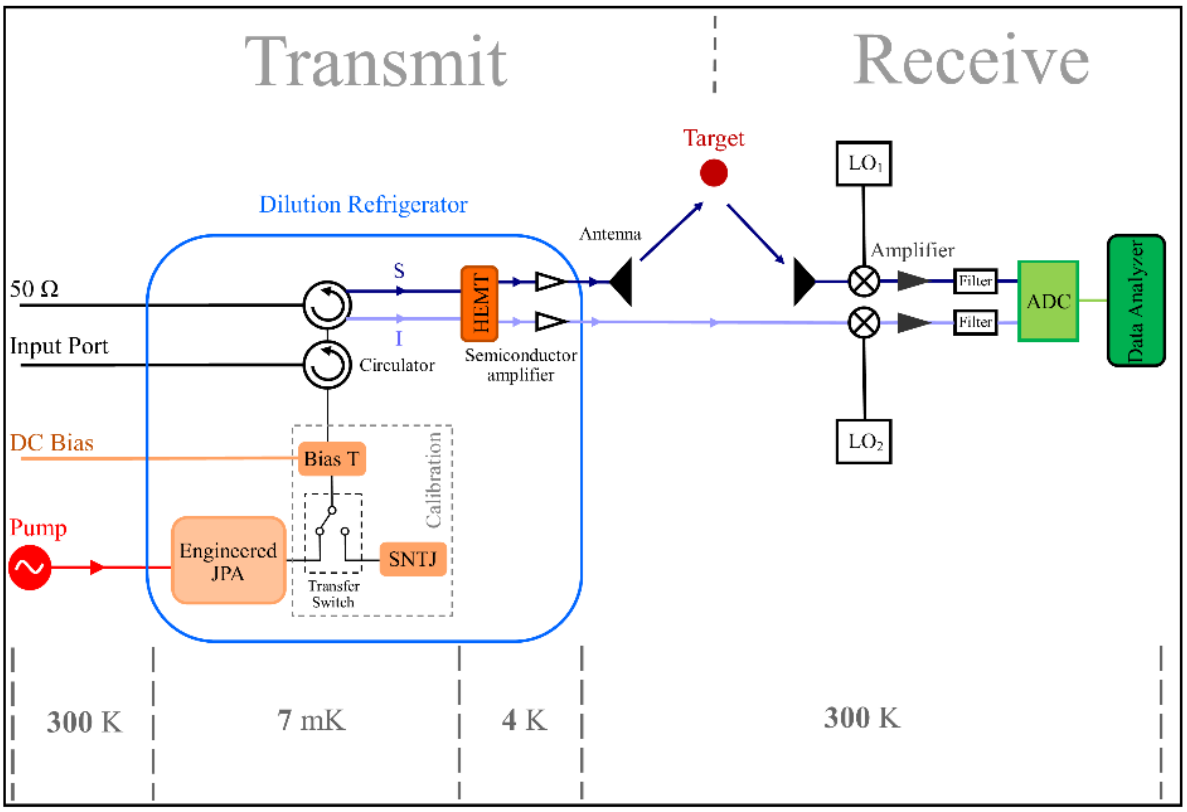


Fig. 4. Block diagram of the QR using EJPA.

After calibration, circulators are placed, which act as insulators for our system to prevent additional signal and noise from reaching the JPA [1-3, 5, 6, 8, 15]. After amplification, the signal is sent to the target by the C-band antenna, but we record the idler. It should be noted that no measurements are made on the idler before the signal arrives. The local oscillators (LO) $LO_1$ and $LO_2$ are applied to the reflection signal of the target and the idler to convert the frequency to the intermediate frequency (20 MHz) [15]. Finally, the signal is amplified again and detected after digitization.

Note that in this work, we don't have a delay line here, but there is a time delay to measure the signal and idler [1]. The two pulses are measured at different times (does not require joint measurement). The time delay between the two pulses is due to the length of the free-space path of the transmitted signal [1].

### 3.3. Post-Processing

The idler and signal modes are recorded after amplification with an analog-to-digital converter (ADC) card (for example, dual-channel ADC AD570JD with 8-bit resolution) [15]. The recorded data from the ADC is split into shorter arrays of copies. To derive the measurement statistics of the signal and idler mode quadratures can be used the digital fast Fourier transform (FFT) at idler ($\omega_1$) and signal frequencies ($\omega_s$) after analog down conversion on each array separately. These measurement results are useful to compute the covariances of the signal and idler modes. Then, two pulses are received with the digital phase-conjugate receiver as shown in Fig. 5. This receiver is used to infer the $SNR^{QR}$ [15].

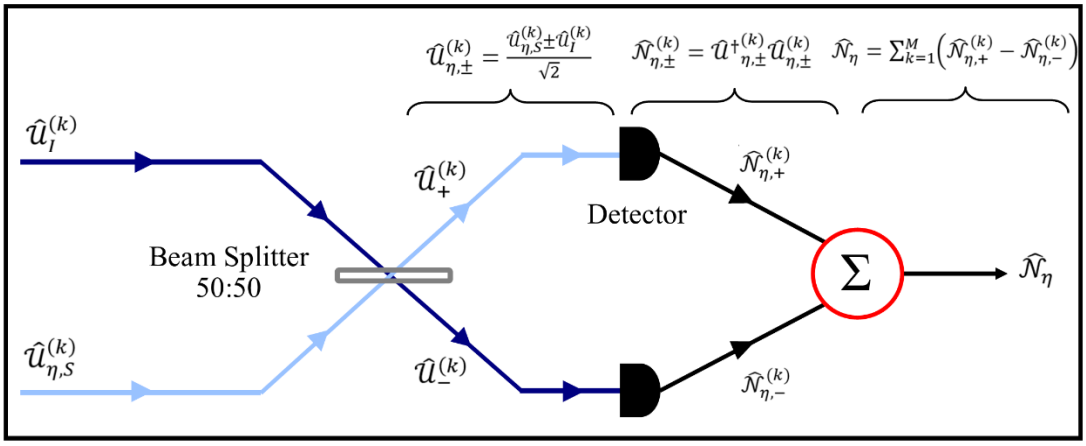


Fig. 5. The post-processing and digital phase-conjugate receiver.

The $M$ copies of the signal and idler modes are sent to the receiver (Fig. 5). The task of the beam splitter (50:50) is to mix the phase-conjugated signal mode reflected from the target, with the locally detected idler mode. The outputs of the beam splitter are detected (that is used as the input to a threshold detector (output is the target absence or presence decision)). According to Fig. 5, $\hat{\mathrm{U}}_{\eta,S}^{(k)}$ (received signal mode $1 \le k \le M$) and $\hat{\mathrm{U}}_I^{(k)}$ (received idler mode $1 \le k \le M$) are mixed by a 50:50 beam splitter and the output is as follows [15, 34]:

$$\hat{\mathrm{U}}_{\eta,\pm}^{(k)} = \frac{\hat{\mathrm{U}}_{\eta,S}^{(k)} \pm \hat{\mathrm{U}}_I^{(k)}}{\sqrt{2}}, \tag{1}$$

After detecting these modes, the photon counts are equal to the quantum measurements of the corresponding number operator [15, 34]:

$$\hat{\mathrm{N}}_{\eta,\pm}^{(k)} = \hat{\mathrm{U}}_{\eta,\pm}^{\dagger(k)} \hat{\mathrm{U}}_{\eta,\pm}^{(k)}, \tag{2}$$

The total photon counts for the two detectors are equal to

$$\hat{\mathrm{N}}_\eta = \sum_{k=1}^{M} \left( \hat{\mathrm{N}}_{\eta,+}^{(k)} - \hat{\mathrm{N}}_{\eta,-}^{(k)} \right). \tag{3}$$

According to the recent literature [34, 15], the microwave mode of the signal return to post-processing ( $\eta = 0$ in the absence of the target and $\eta \neq 0$ in the presence of the target) is equal to [34, 15]:

$$\hat{\mathrm{U}}_{\eta,S}^{(k)} = \sqrt{G_s}\left[\sqrt{\eta}\hat{a}_S + \sqrt{\frac{\eta\left(G_s^A - 1\right)}{G_s^A}}\hat{a}_{n,S}^{\dagger A} + \sqrt{\frac{(1-\eta)}{G_s^A}}\hat{a}_n^E + \sqrt{\frac{\left(G_s^A - 1\right)}{G_s}}\hat{a}_{n,S}^{\dagger D}\right] + \sqrt{2}\hat{a}_V \,, \tag{4}$$

As well, the idler's microwave mode toward the post-processor

$$\hat{\mathrm{U}}_I^{(k)} = \sqrt{G_I}\left[\hat{a}_I + \sqrt{\frac{\left(G_I^A - 1\right)}{G_I^A}}\hat{a}_{n,I}^{\dagger A} + \sqrt{\frac{\left(G_I^A - 1\right)}{G_I}}\hat{a}_{n,I}^{\dagger D}\right]. \tag{5}$$

Here $G_s = G_s^D\left(dB\right)G_s^A\left(dB\right)$ is the system signal gain where $G_s^D$ and $G_s^A$ are the detection signal gain and amplification signal gain, respectively. Also $G_I = G_I^D\left(dB\right)G_I^A\left(dB\right)$ is the system idler gain. The effective dissipation range is $-25dB < \eta < 0dB$. $\hat{a}_S$ and $\hat{a}_I$ are the signal and idler annihilation operators, respectively. $\hat{a}_{n,S}^{\dagger A}$ and $\hat{a}_{n,I}^{\dagger A}$ are the signal and idler amplification noise creation operators at 4 K, respectively. $\hat{a}_n^E$ is the environment noise mode operator at room temperature and $\hat{a}_V$ is the vacuum mode. $\hat{a}_{n,S}^{\dagger D}$ and $\hat{a}_{n,I}^{\dagger D}$ are the signal and idler detection creation operators at 290 K, respectively [15, 34].

The error probability is obtained in two parts corresponding to the absence or presence of the target (the false-alarm probability $P_f$ and the miss probability $P_r$). The error probability in quantum receivers is [15, 34-45]:

$$P_{D(M)}^{QR} = \frac{P_f + P_m}{2} = \frac{erfc\left[\sqrt{\left(SNR\right)_M^{QR}/8}\right]}{2}. \tag{6}$$

The detection probability in terms of the false-alarm probability for QTMS radar according to previous publications [1-3, 5, 6, 8, 32, 33], is expressed by:

$$P_D^{QR} = Q_1\left(\frac{\rho\sqrt{2N}}{1-\rho^2}, \frac{\sqrt{-2lnP_{FA}}}{1-\rho^2}\right), \tag{7}$$

where $N$ is the number of channels, $Q_1$ is the Marcum function [34] and $\rho$ is quantum correlation coefficient [35-45]:

$$\rho = \frac{\rho_0}{\sqrt{1+\left(1/\,SNR^{QR}\right)^4}}. \tag{8}$$

where the $SNR^{QR}$ is the signal-to-noise ratio of QTMS radar and is defined as [15, 34, 36, 37]:

$$(SNR)_M^{QR} = \frac{4M\left[\left(\left\langle \hat{N}_{\eta,+}\right\rangle_{H_1} - \left\langle \hat{N}_{\eta,-}\right\rangle_{H_1} - \left(\left\langle \hat{N}_{\eta,+}\right\rangle_{H_0} - \left\langle \hat{N}_{\eta,-}\right\rangle_{H_0}\right)\right)\right]^2}{\left(\sqrt{\left\langle \Delta\hat{N}_{\eta}^{\,2}\right\rangle_{H_0}} + \sqrt{\left\langle \Delta\hat{N}_{\eta}^{\,2}\right\rangle_{H_1}}\right)^2} \tag{9}$$

Here $M = B.\tau$ is the number of modes, $B$ is the bandwidth, and $\tau$ is the time. Also, the value expected indicates the average over the total $M$ copy. The terms in the above equation are expressed in "Supplementary Material".

### 3.4. Simulation

In this study, we used C-band antennas (4-8 GHz). These antennas have fewer losses than X-band antennas (8-12 GHz) [1-3]. System parameters are calculated in Table I, to compare with the corresponding parameters obtained from the information reported in [1] and [15], as follows:

TABLE I: The calculated parameters of QTMS radar. * Calculated parameters based on the results reported in [15]. † Calculated parameters based on the results reported in [1]. ‡ Parameters used from [22].

| Quantity | EJPA [This work] | JRM [15] | JPA [1] | Unit |
|---|---|---|---|---|
| Antenna | C-band | X-band | X-band | --- |
| Antenna gain (G) | 6.4 | 15* | 15 | dB |
| Antenna effective area ($A_e$) | $8.8 \times 10^{-5}$ | ---- | ---- | $m^2$ |
| Target radar cross-section ($\sigma$) | 1.0 | ---- | ---- | $m^2$ |
| Bandwidth (B) | 300‡ | 20 | 1.0 | MHz |
| JPA or JPC power gain ($G_p$) | 20 | 30 | 20† | dB |
| HEMT gain (at 4 K) ($G_{HEMT}$) | 38 | 36 | 36† | dB |
| Signal gain ($G_S$) | 83.98 | 93.98 | ~96† | dB |
| Detection gain ($G^D$) | 16.82 | 16.82 | 16.82† | dB |
| Amplifier gain ($G^A$) | 67.16 | 77.16 | 79.18† | dB |
| Signal power ($P_s$) | 5‡ | -128* | -82 | dBm |
| Pump power ($P_p$) | 6‡ | -97 | ----- | dBm |
| Noise power ($P_n$) | -145 | 4 | -94 | dBm |
| Pump frequency $\omega_p = \omega_s + \omega_i$ | 10.62 | 16.89 | 13.6821† | GHz |
| Signal frequency ($\omega_s$) | 5.31 | 10.09 | 6.1445 | GHz |
| Idler frequency ($\omega_i$) | 5.31 | 6.8 | 7.5376 | GHz |
| Signal-to-noise ratio ($SNR^{QR}$) | -13.48 | -18 | -19 | dB |
| Range (R) ($N_s = 0.1$ and $\eta = 1$ dB ) | 482 with signal transmission to target | 1 with signal transmission to target (short-range) | 0.5 without signal transmission to target | m |

### 3.4.1. SNR and ROC

Using Eqs. (9 and (Eqs. (11-18) in the appendix)), Fig. 6 shows the SNR versus $N_s$ plot comparing the three scenarios: conventional JPA (the latest version of the QTMS radar) [1,3], Josephson ring modulators (JRM) [15], and EJPA. The clear conclusion that can be deduced from this plot is that the SNR performs better in the EJPA scenario than in the other scenarios. The SNR for EJPA is about 5 dB better than JRM, and about 6 dB better than conventional JPA. Therefore, the EJPAs are promising to improve SNR, meaning a better performance of quantum radars. It means that we

have a 6 dB improvement of SNR, in addition to an improvement of 4 to 6 dB (latest version of QTMS radar [1]) in SNR in the previous works [2-9, 15, 19, 20].

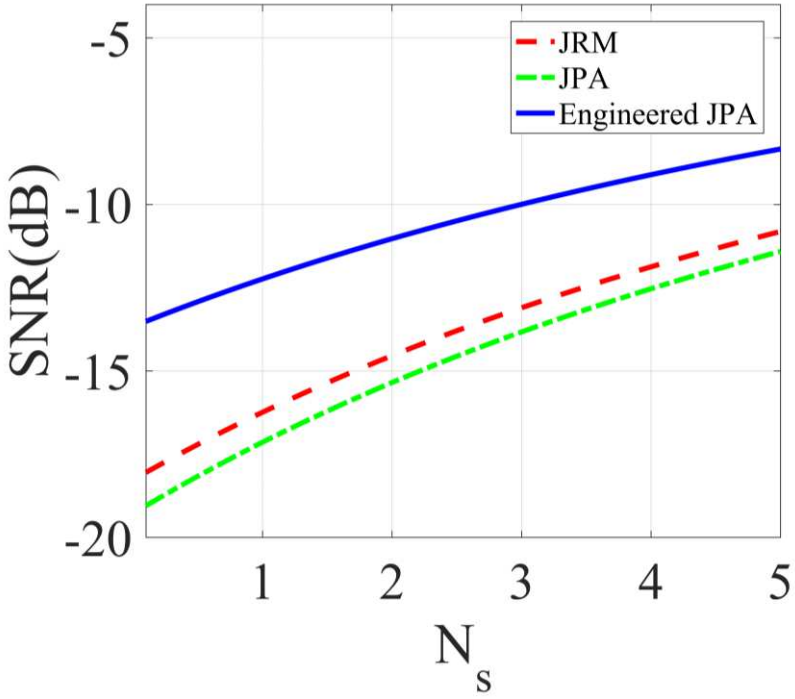


Fig. 6. Comparison of SNRs for conventional JPA, JRM, and EJPA versus $N_s$.

Using Eq. (23), the ROC diagram for different scenarios is depicted in Figs 7 and 8, which clearly show the superiority of the EJPA compared to other scenarios. In Fig. 7, the probability of detection in EJPA is better than in other scenarios.

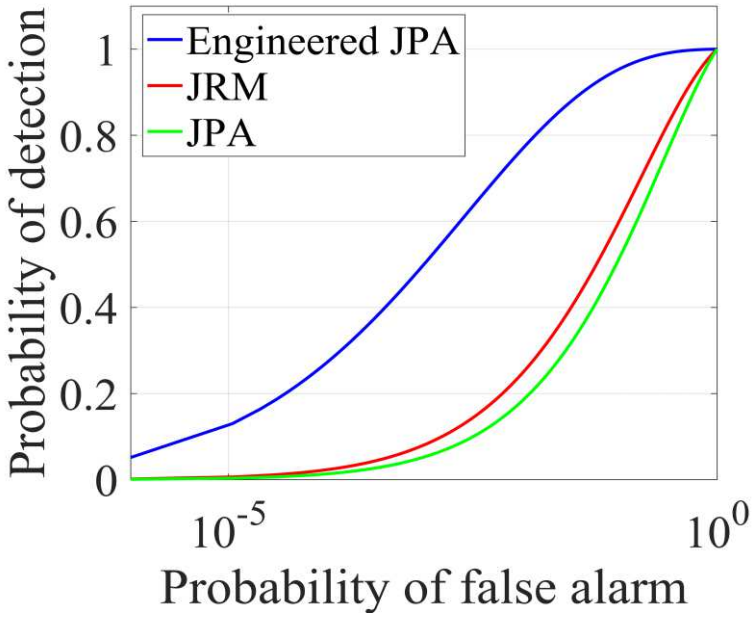


Fig. 7. The ROC comparison plot. Comparison between conventional JPA (green), JRM (red) and EJPA (blue), for $N_s$=0.1, $N$=150 and $\rho_0$=1.

The ROC comparison plot for conventional JPA, JRM, and EJPA is illustrated in Fig. 8. It is clear that the detection probability in an EJPA with a smaller number of N channels reaches a maximum of one, demonstrating a significant improvement.

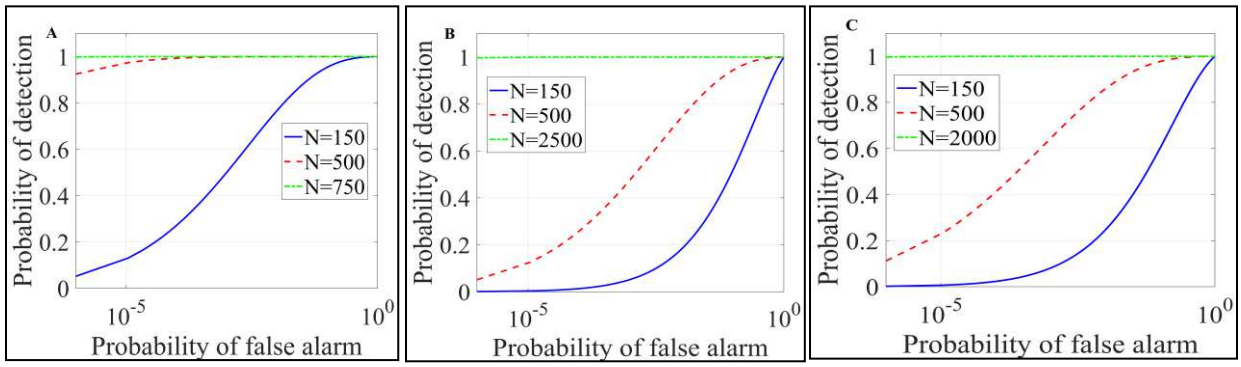


Fig. 8. The ROC comparison plots, EJPA (A), conventional JPA (B), and JRM (C); with different channel numbers N.

The SNR plot is also examined versus a correlation function in Fig. 9 (A). This figure shows that when the correlation increases, the SNR of the QTMS radar also increases. Therefore, the correlation and entanglement play the most important role in QTMS radars and we need to fabricate more correlated signal and idler (by engineering the JPAs) [37-45]. In this model, the qualitative behavior of the correlation function shows that increasing the bandwidth does not suppress the correlation, as is shown in Fig. 9 (B).

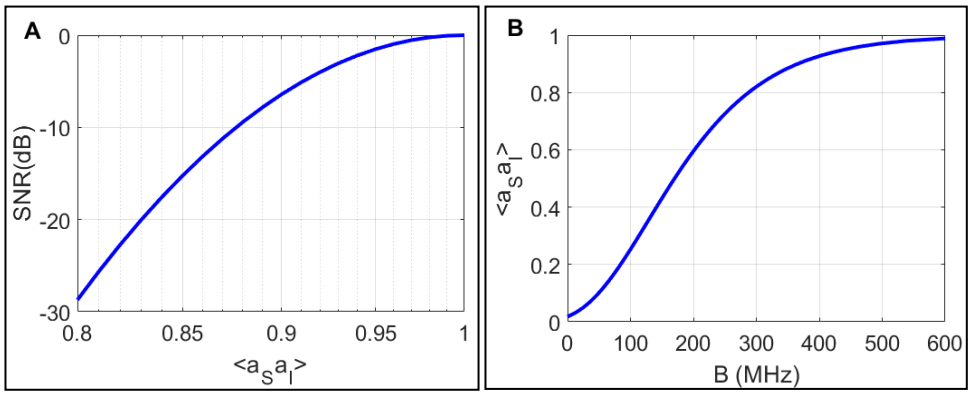


Fig. 9. SNR plot as a correlation function for an EJPA (A), and (B) correlation function in terms of bandwidth B(MHz).

### 3.4.2. QTMS Radar Range

As mentioned earlier, range evaluation is one of the most important tasks of the quantum radar. Since QTMS radars are very similar to conventional noise radars, the QTMS range equation would be as follows [35, 46, 47]:

$$R_{max} = \left( \frac{G A_e \sigma P_s}{(4\pi)^2 P_n (SNR)^Q_{min}} \right)^{1/4} . \qquad (10)$$

where $G$ is the antenna gain, λ is the wavelength, $A_e = G\lambda^2 / 4\pi$ is the effective antenna area, σ is the target radar cross-section, $P_s$ and $P_n$ are the signal and noise power respectively. The only difference between this equation and the conventional noise radar equation is $(SNR)^Q_{min}$, which is

SNR of QTMS radar here. Fig. 10 depicts the detection range versus $(SNR)_{min}^{Q}$. It is clear that the range in EJPA (with signal transmission to the target) has a remarkable increase from 0.5 m in conventional JPA (with signal transmission to the target (for short-range)) [1-3], and 1 m in JRM (One-way without signal transmission to the target) [15], to several hundred meters (482 m). Additionally, SNR loses performance efficiency with increasing range.

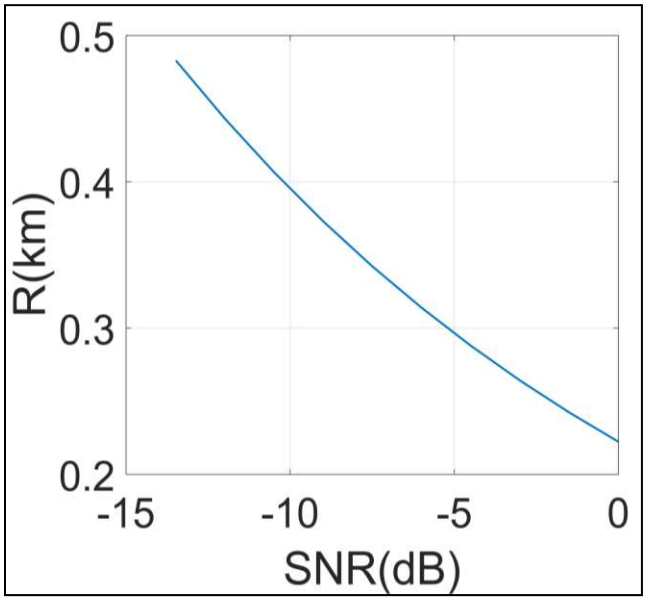


Fig. 10. Detection range versus SNR of EJPA.

## 4. Conclusion

In this study, a proposed QTMS (quantum two-mode squeezed) radar based on an EJPA (engineered Josephson parametric amplifier) quantum source, was designed and simulated and its performance was evaluated and compared to two other radar scenarios: the conventional JPA quantum source (latest version of QTMS radar) [1], and Josephson ring modulator (JRM) [15]. The application of an EJPA in QTMS radar leads to a significant overall improvement in radar performance. The correlation between the signal and idler is the most substantial part of QR. The

more the correlation, the performance of QR can be better. Therefore, we must fabricate JPAs that can generate signals and idlers with much higher correlations (by engineering the JPAs). From our findings, the SNR of the QTMS radar shows a performance efficiency of about 5 dB relative to the JRM [15] and about 6 dB relative to the conventional JPA (it means that the QTMS radar has shown much more enhancement from CR than 6 dB [2-9, 15, 19, 20], and this study purports to have an additional 6 dB from those results [1]). The detection probability is also remarkably higher than the other two considered scenarios. Moreover, our channel numbers in the detection probability are much less, compared with the other two scenarios. Furthermore, the QTMS radar range equation was defined, and it was expressed that as the QTMS radar range increases, the SNR of QTMS radar decreases proportionally. In the previous works [1,3,15] for QTMS radar, the signal was not transmitted to the target [1, 3] and only the transmitter and receiver antennas were facing each other, also in [15], low-power short-range radar (1 m due to low power). However, in our work, the signal transmission to the target for long-range was simulated. Finally, we transmit the signal to the target and obtained a remarkable increase of 482 m for the QTMS radar range in EJPA (with signal transmission to the target), compared to one meter in the JRM and half a meter in the conventional JPA (latest version of the QTMS radar). Therefore, we confirmed that using the EJPA in QTMS radar, is very promising to get a considerable improvement in radar performance.

## Acknowledgement

The authors would like to thank J. Teixeira for helping with the manuscript and valuable comments.

# References


[1] Luong, D., Chang, C. W. S, Vadiraj, A. M., Damini, A., Wilson, C. M. & Balaji, B. Receiver operating characteristics for a prototype quantum two-mode squeezing radar. *IEEE Trans. Aerosp. Electron. Syst.* **56**, 2041-2060 (2019).

[2] Chang, C. S., Vadiraj, A. M., Bourassa, J., Balaji, B. & Wilson, C. M. Quantum-enhanced noise radar. *Appl. Phys. Lett.* **114**, 112601 (2019).

[3] Luong, D., Balaji, B., Chang, C.W. S., Rao, V. M. A. & Wilson, C. M. Microwave quantum radar: An experimental validation. *In 2018 International Carnahan Conference on Security Technology (ICCST)*, (IEEE, 2018), pp. 1-5.

[4] Shapiro, J. H. The quantum illumination story. *IEEE Trans. Aerosp. Electron. Syst. Magazine.* **35**, 8-20 (2020).

[5] Luong, D., Rajan, S. & Balaji, B. Quantum Monopulse Radar. *In 2020 International Applied Computational Electromagnetics Society Symposium (ACES)*, (IEEE, 2020), pp. 1-2.

[6] Luong, D., Rajan, S. & Balaji, B. Entanglement-based quantum radar: From myth to reality. *IEEE Trans. Aerosp. Electron. Syst. Magazine* **35**, 22-35 (2020)

[7] Liu, H., Helmy, A. & Balaji, B. Inspiring radar from quantum-enhanced LiDAR. *In 2020 IEEE International Radar Conference (RADAR)*, (IEEE, 2020), pp. 964-968.

[8] Luong, D., Rajan, S. & Balaji, B., Are quantum radar arrays possible?. *In 2019 IEEE International Symposium on Phased Array System & Technology (PAST)*, (IEEE, 2019), pp. 1-4.

[9] Luong, D. & Balaji, B. Quantum radar, quantum networks, not-so-quantum hackers. *In Signal Processing, Sensor/Information Fusion, and Target Recognition XXVIII, vol.* **11018**. *International Society for Optics and Photonics*, (2019), p. 110181E.

[10] Frasca, M. & Farina, A., Multiple Input-Multiple Output Quantum Radar. *In2020 IEEE Radar Conference (RadarConf20)*, (IEEE, 2020) pp. 1-4.

[11] Daum, F. Quantum radar cost and practical issues. *IEEE Trans. Aerosp. Electron. Syst. Magazine* **35**, 8-20 (2020).

[12] Daum, F. A system engineering perspective on quantum radar. *In 2020 IEEE International Radar Conference (RADAR)*, (IEEE, 2020), pp. 958-963.

[13] Torromé, R. G., Bekhti-Winkel, N. B. & Knott, P. Introduction to quantum radar, arXiv:2006.14238.

[14] Barzanjeh, S., Guha, S., Weedbrook, C., Vitali, D., Shapiro, J. H. & Pirandola, S. Microwave quantum illumination. *Phys. Rev. Let*t. **114**, 080503 (2015).

[15] Barzanjeh, S., Pirandola, S., Vitali, D. & Fink, J. M. Microwave quantum illumination using a digital receiver. *Sci. Adv.* **6**, eabb0451 (2020).

[16] Maccone, L. & Ren, C. Quantum radar. *Phys. Rev. Lett.* **124**, 200503 (2020).

[17] Pirandola, S., Bardhan, B. R., Gehring, T., Weedbrook, C. & Lloyd, S. Advances in photonic quantum sensing. *Nat. Photonics* **12**, 724-733 (2018).

[18] Tan, S-H, Erkmen, B. I., Giovannetti, V., Guha, S., Lloyd, S., Maccone, L., Pirandola, S. & Shapiro, J. H. Quantum illumination with Gaussian states. *Phys. Rev. Lett.* **101**, 253601 (2008).

[19] Liu, H., Balaji, B. & Helmy, A. S. Target detection aided by quantum temporal correlations: theoretical analysis and experimental validation. *IEEE Trans. Aerosp. Electron. Syst.* **56**, 3529-3544, (2020).

[20] Zhuang, Q. & Shapiro, J. H. Ultimate accuracy limit of quantum pulse-compression ranging. *Phys. Rev. Lett.* **128**, 1010501 (2022).

[21] Lanzagorta, M. Quantum radar. *Synthesis Lectures on Quantum Computing* **3**, 1-139 (2011).

[22] Grebel, J., Bienfait, A., Dumur, É., Chang, H-S., Chou, M-H., Conner, C. R., Peairs, G. A., Povey, R. G., Zhong, Y. P. & Cleland, A. N. Flux-pumped impedance-engineered broadband Josephson parametric amplifier. *Appl. Phys. Lett.* **118**, 142601 (2021).

[23] Barnett, S. & Radmore, P. M. Methods in theoretical quantum optics. Vol. 15. Oxford University Press, 2002.

[24] Nielsen, M. A. & Chuang, I. Quantum computation and quantum information. 558-559 (2002).

[25] Zubairy, M. S. Quantum state measurement via Autler-Townes spectroscopy. *Phys. Lett. A* **222**, 91-96 (1996).

[26] Nakahara, M. Quantum computing: from linear algebra to physical realizations. CRC Press, 2008.

[27] Weedbrook, C., Pirandola, S., Thompson, J., Vedral, V. & Gu, M. How discord underlies the noise resilience of quantum illumination. *New J. Phys*. **18**, 043027 (2016).

[28] Salmanogli, A. & Gokcen, D., Entanglement sustainability improvement using optoelectronic converter in quantum radar (interferometric object-sensing). *IEEE Sens. J.* **21**, 9054-9062 (2021).

[29] Salmanogli, A., Gokcen, D. & Gecim, H. S. Entanglement sustainability in quantum radar. *IEEE J. Sel. Top. Quantum Electron.* **26**, 1-11 (2020).

[30] Xiangbin, W., Hiroshima, T., Tomita, A. & Hayashi, M. Quantum information with Gaussian states. *Phys. Rep.* **448**, 1-11 (2007).

[31] Sebastian, K., Storz, S., Kurpiers, P., Magnard, P., Heinsoo, J., Keller, R., Luetolf, J., Eichler, C. & Wallraff, A. Engineering cryogenic setups for 100-qubit scale superconducting circuit systems. *EPJ Quantum Technol.* **6**, (1) 2 (2019).

[32] Luong, D. & Balaji, B. Quantum two-mode squeezing radar and noise radar: covariance matrices for signal processing. *IET Radar, Sonar & Navigation* **14**, 97-104 (2020).

[33] Luong, D., Rajan, S. & Balaji, B. Quantum two-mode squeezing radar and noise radar: Correlation coefficients for target detection. *IEEE Sens. J.* **20**, 5221-5228 (2020).

[34] Cai, Q., Liao, J., Shen, B., Guo, G. & Zhou, Q. Microwave quantum illumination via cavity magnonics. *Phys. Rev. A* **103**, 052419 (2021).

[35] Luong, D., Balaji, B. & Rajan, S. Performance prediction for coherent noise radars using the correlation coefficient. *IEEE Access* **10**, 8627-8633 (2022).

[36] Braunstein, S. L. & Loock, P. V. Quantum information with continuous variables. *Rev. Mod. Phys.* **77**, 513 (2005).

[37] Cai, Q., Liao, J. & Zhou, Q. Stationary entanglement between light and microwave via ferromagnetic magnons. *Annalen der Physik* **532**, 2000250 (2020).

[38] Barzanjeh, S., Redchenko, E. S., Peruzzo, M., Wulf, M., Lewis, D. P., Arnold, G. & Fink, J. M. Stationary entangled radiation from micromechanical motion. *Nature* **570**, 480-483 (2019).

[39] Li, J. & Gröblacher, S. Entangling the vibrational modes of two massive ferromagnetic spheres using cavity magnomechanics. *Quantum Sci. Technol.* **6**, 024005 (2021).

[40] Weedbrook, C., Pirandola, S., García-Patrón, R., Cerf, N. J., Ralph, T. C., Shapiro, J. H. & Lloyd, S. Gaussian quantum information. *Rev. Mod. Phys.* **84**, 621 (2012).

[41] Vidal, G. & Werner, R. F. Computable measure of entanglement. *Phys. Rev. A* **65**, 032314 (2002).

[42] Plenio, M. Logarithmic negativity: a full entanglement monotone that is not convex. *Phys. Rev. Lett.* **95**, 090503 (2005).

[43] Boura, H. A. & Isar, A. Logarithmic negativity of two bosonic modes in the two thermal reservoir model. *Rom. J. Phys.* **60**, 1278 (2015).

[44] Wang, X. & Wilde, M. M. α-logarithmic negativity. *Phys. Rev. A* **102**, 032416 (2020).

[45] Salmanogli, A., Gokcen, D. & Gecim, H. S. Entanglement of optical and microcavity modes by means of an optoelectronic system. *Phys. Rev. Appl.* **11**, 024075 (2019).

[46] Mahafza, B. R., Radar systems analysis and design using MATLAB. Chapman and Hall/CRC, 2005.

[47] Mahafza, B. R. Radar signal analysis and processing using MATLAB. Chapman and Hall/CRC, 2016.

## Author contributions

Practical research was conducted by M.N. and S.M.H. and M.H.G. Interpretations and comparison of results and writing of the article were done by M.N., S.M.H. with help of J.S.Y. The article was reviewed and edited by J.S.Y.

## Competing interests

The authors declare no competing interests.

## Data availability statement

All data generated or analysed during this study are included in this published article [and its supplementary information files].

## Additional information

Correspondence and requests for materials should be addressed to J.S.Y. and S.M.H.